

# Hydroprocessing of furfural over in situ generated nickel phosphide based catalysts in different solvents

Maria A. Golubeva\*, Anton L. Maximov

A.V.Topchiev Institute of Petrochemical Synthesis, RAS, Moscow, 119991, Russian Federation

## ARTICLE INFO

### Keywords:

Nickel phosphide  
Furfural  
Bio-oil  
Hydrodeoxygenation  
Dispersed catalysts

## ABSTRACT

The present work is dedicated to the nickel phosphide based catalysts, containing particles, generated in situ in the reaction medium from the different catalytic systems. The present catalytic systems exhibited high activity in the hydroprocessing of furfural. Full conversion of furfural depending on conditions was reached after 0.5–3 hours of reaction at 250–350 °C. 2-methylfuran was obtained as a main product in toluene with the highest selectivity of 77 %. Ethyl levulinate and 2-methylfuran with selectivity of 40 % and 38 % respectively were obtained as main products in ethanol under different conditions. Different reaction medium and nickel phosphide precursors had an influence on the obtained phases of catalysts. Ni<sub>12</sub>P<sub>5</sub> and Ni<sub>2</sub>P were obtained in toluene from oil-soluble precursors and Ni<sub>12</sub>P<sub>5</sub> was obtained in ethanol from water-soluble precursors.

## 1. Introduction

Nowadays, the whole world community is interested in alternative energy sources, such as renewable sources. Especially it can be produced everywhere, where agriculture, food and wood industry are developed. Over the past fifteen years biofuel production greatly increased and various biofuel regulation standards appeared. The leading countries in the production of biofuels are the USA, Germany and France [1]. A feedstock for biofuel production is biomass. About 200 billion tonnes of biomass are formed every year around the world [2,3]. Biomass consists of different types of polymers such as cellulose (38–50 %), hemicellulose (23–32 %) and lignin (15–25 %) [3]. Hemicellulose is the second spread polysaccharide available in nature [3,4]. Such hemicellulose-derived compound as furfural deserves much attention as a perspective platform for chemicals and biofuels. According to various estimates, annual production of furfural is between 300 and 800 thousand tonnes [5]. Using various types of catalysts, furfural can be converted to different promising components of biofuels such as furans and their tetrahydro-derivatives, furfuryl alcohol, tetrahydrofurfuryl alcohol, levulinic acid and its esters [4,6],  $\gamma$ -valerolactone [4,7] and others.

Noble metals and transition metal sulfides are generally used in hydrodeoxygenation (HDO), but both types of catalysts have some disadvantages. Noble metals are characterized by high price and transition metal sulfides additionally need a sulfiding agent. Interesting alternative catalysts are transition metal phosphides. In recent years, this class of

catalysts has attracted much attention due to the wide range of applications, including the field of catalysis [8,9]. Various methods of phosphides synthesis exist. The most commonly used is temperature-programmed reduction (TPR) of phosphate precursors [9–12]. It is a simple technique, however, reduction temperature is high enough [12]. Low temperature synthesis methods are also known. They include the application of phosphorus sources, where phosphorus is in lower oxidation state. For example, phosphorous H<sub>3</sub>PO<sub>3</sub> and hypophosphorous H<sub>3</sub>PO<sub>2</sub> acids or their salts and various organic phosphines PR<sub>3</sub> (R = phenyl, butyl, octyl etc.) are related to such sources [10,13].

We proposed a method for producing phosphide-based catalysts from different precursors during hydroprocessing of various substrates. This approach is that the active phase of the catalyst forms independently in a reactor in parallel with the process of the substrate hydroprocessing. In this case, pre-synthesis of the catalyst is avoided. The using of the catalytic systems allows nickel phosphide to form in situ in the reaction medium. Previously, this approach has been successfully worked out in the hydrodeoxygenation of guaiacol (bio-oil phenolic compound) [14], palmitic and stearic acids [15]. In present work, this approach was applied to hydrodeoxygenation of furfural. The first catalytic system contained oil-soluble compounds such as Ni (II) 2-ethylhexanoate, tri-octylphosphine (TOP), toluene and furfural. The second catalytic system contained water-soluble compounds such as Ni (II) acetate, hypophosphorous acid, ethanol and furfural.

Previously, furfural hydrodeoxygenation over nickel phosphide

\* Corresponding author at: A.V.Topchiev Institute of Petrochemical Synthesis, RAS, Leninsky pr., 29, Moscow, 119991, Russian Federation.  
E-mail address: [vinnikova@ips.ac.ru](mailto:vinnikova@ips.ac.ru) (M.A. Golubeva).

<https://doi.org/10.1016/j.apcata.2020.117890>

Received 16 September 2020; Received in revised form 14 October 2020; Accepted 15 October 2020

Available online 23 October 2020

0926-860X/© 2020 Elsevier B.V. All rights reserved.

based catalysts was studied in several works (Table 1). 2-methylfuran [16–19], furan [18], furfuryl alcohol [20], 2-pentanol [19], 2-propoxy-methylfuran [19] were obtained as main products. In present work, 2-methylfuran was obtained with 77 % of selectivity at full conversion of furfural using toluene as a solvent and the catalytic system, containing nickel phosphide, whereas in other works the similar conversion and 2-methylfuran selectivity reached under gas-phase reaction conditions [18], using 2-propanol [16,17,19] or cyclopentyl methyl ether [18] as solvents. Moreover, in present work, ethyl levulinate and 2-methylfuran

were obtained with 40 % and 38 % of selectivity respectively at full conversion of furfural using ethanol as a solvent and the catalytic system, containing nickel phosphide. Thus, we reached the similar to literature mentioned results in furfural HDO over nickel phosphide based catalysts, using toluene as a solvent and reached different results, using ethanol as a solvent. This influence on the reaction products has not only by the solvent, but also by the use of different catalytic systems including the use of hypophosphorous acid as a precursor.

## 2. Experimental

### 2.1. Materials

Nickel (II) acetate tetrahydrate (Sigma-Aldrich, 98 %), nickel (II) 2-ethylhexanoate (Aldrich, 78 wt.% in 2-ethylhexanoic acid), hypophosphorous acid (Sigma-Aldrich, 50 wt.% in H<sub>2</sub>O), trioctylphosphine (Acros Organics, 90 %) were used for catalysts preparation. Nickel phosphide (Aldrich, 100 mesh, 98 %) was used as a comparative catalyst. Furfural (Component-reaktiv, >99 %) was used as a substrate in hydrogenation, toluene (Component-reaktiv, >99 %) and ethanol (Reakhim, >99 %) were used as solvents. Deionized water and hexane (Component-reaktiv, >99 %) were used for washing the catalysts. Potassium manganite (VII) (Component-reaktiv, ≥98 %) and gases H<sub>2</sub> (Air Liquide, ≥98 %), Ar (Air Liquide, ≥98 %) also were used. Furfural was purified by standard technique before catalytic tests. Ethanol was dried with 3 Å molecular sieves (Sigma-Aldrich, pellets, 3.2 mm). Other reagents were used as received without extra purification.

### 2.2. Catalysts preparation and activity tests

Nickel phosphide catalysts were prepared in a stainless-steel batch reactor during the catalytic tests. Catalysts were prepared using two different types of precursors (water-soluble and oil-soluble) and solvents. The mixture of 23.9 mg of Ni(OAc)<sub>2</sub> (or 41.6 mg of nickel (II) 2-ethylhexanoate) and 24.8 mg of H<sub>3</sub>PO<sub>2</sub> (or 77.4 mg of TOP) with P/Ni molar ratio = 2 and 7 wt. % solution of 225.8 mg of furfural (substrate/Ni molar ratio = 25) in 3 g of ethanol (or toluene) was put in the reactor. The initial pressure of H<sub>2</sub> was 5 MPa. The reactor was heated up to 250–350 °C during 0.5–6 hours with magnetic stirring. After the catalytic tests the reactor was cooled at the room temperature and the gas pressure was released into potassium manganite (VII) solution to remove phosphine residues [21]. Liquid products were isolated from the reactor and were separated from catalyst by centrifugation (5000 rpm). Obtained catalysts were called NiP-H<sub>3</sub>PO<sub>2</sub> and NiP-TOP respectively. The NiP-H<sub>3</sub>PO<sub>2</sub> was washed by water and the NiP-TOP was washed by hexane to dissolve probable residues of water-soluble and oil-soluble precursors respectively. Catalysts were dried in an oven at 120 °C and were kept under Ar.

All experiments with purchased nickel phosphide and recycling tests of catalysts were carried out at the reaction conditions mentioned above. For the comparative study 7.1 mg of nickel phosphide was used.

### 2.3. Characterization

Liquid products were analyzed by gas chromatography with flame-ionization detector (GC–FID) and gas chromatography–mass spectrometry (GC–MS). Qualitative analysis of liquid products was carried out using a Thermo Focus DSQ II instrument with a capillary column Varian VF-5MS (30 m x0.25 mm x0.25 μm) and helium as a carrier gas. The components were identified using reference mass spectra of the NIST/EPA/NIH database. Quantitative analysis of liquid products was carried out using a gas-liquid chromatograph Crystallux 4000 M with a flame ionization detector, a capillary column SPB-1 (Superlco, 30 m x0.25 mm x0.25 μm), helium as a carrier gas. To obtain and analyze chromatograms NetChromWin software was used. Furfural conversion and products yields were calculated using the following equations:

**Table 1**

Literature reported results of furfural HDO over NiP-based catalysts.

Catalyst	Reaction conditions	Conversion, %	Selectivity, %	Reference
Ni <sub>2</sub> P (Ni <sub>2</sub> P-0.5*)	240 °C, 2 MPa H <sub>2</sub> , 4 h, 0.1 g cat., 0.5 ml of furfural in 3 ml of 2- propanol	100	83.1 for 2- methylfuran	[16]
Ni <sub>2</sub> P (Ni <sub>2</sub> P-1.00–300*)	260 °C, 1.5 MPa H <sub>2</sub> , 3 h, 0.1 g cat., 0.5 ml of furfural in 3 ml of 2- propanol	100	91.2 for 2- methylfuran	[17]
15 wt.% Ni <sub>2</sub> P/SiO <sub>2</sub> (Ni <sub>2</sub> P-15-2*)	210 °C, H <sub>2</sub> flow =10 ml/min, feed flow =2.3 mmol furfural/h, 1 h of TOS, 0.15 g cat,	100	75.4 for 2- methylfuran	[18]
15 wt.% Ni <sub>2</sub> P/SiO <sub>2</sub> (Ni <sub>2</sub> P-15-3*)	5 vol.% of furfural in cyclopentyl methyl ether 310 °C, 2 MPa H <sub>2</sub> , H <sub>2</sub> flow =50 ml/ min, WHSV =1.98 h <sup>-1</sup> , 2.5 wt. % of furfural in 2- propanol	92.4	66.5 for furan	
NiPMoS	230 °C, 2 MPa H <sub>2</sub> , H <sub>2</sub> flow =50 ml/ min, WHSV =1.98 h <sup>-1</sup> , 2.5 wt. % of furfural in 2- propanol	95.1	57.7 for 2- methylfuran	
15 wt.% NiPMoS/ laponite	230 °C, 2 MPa H <sub>2</sub> with H <sub>2</sub> flow =50 ml/min, WHSV =1.98 h <sup>-1</sup> , 2.5 wt.% of furfural in toluene	98.1	67.4 for 2- propoxy methyl furan	[19]
Ni <sub>85</sub> P <sub>15</sub>	80 °C, 1.7 MPa H <sub>2</sub> , 4 h, 0.3 g. cat., 2 ml of furfural in 170 ml of ethanol	50	80 for furfuryl alcohol	[20]
	250 °C, 5 MPa, 3 h, furfural/Ni = 25; 225.8 mg of furfural in 3 g of toluene		44 for furan	
	350 °C, 5 MPa, 6 h, furfural/Ni = 25; 225.8 mg of furfural in 3 g of toluene		77 for 2- methylfuran	
NiP-based catalyst	350 °C, 5 MPa, 3 h, furfural/Ni = 25; 225.8 mg of furfural in 3 g of ethanol	100	40 for ethyl levulinate	This work
	350 °C, 5 MPa, 1 h, furfural/Ni = 25; 225.8 mg of furfural in 3 g of ethanol		38 for 2- methylfuran	

\* The name of the catalyst in the article.

$$\text{Conversion (\%)} = \frac{\text{mole of consumed substrate}}{\text{initial mole of substrate}} \times 100\%$$

$$\text{Yield (\%)} = \frac{\text{mole of formed product}}{\text{initial mole of substrate}} \times 100\%$$

The crystalline phases of catalysts were detected by X-ray diffraction (XRD) analysis, which was carried out using a Rigaku Rotaflex RU-200 diffractometer ( $\text{CuK}\alpha$  radiation) in the range of  $5\text{--}100^\circ 2\theta$ , with a goniometer (Rigaku D/Max-RC), a rotation speed of  $1^\circ 2\theta/\text{min}$ , a step  $0.04^\circ$ . Qualitative phase analysis of the samples was carried out using the PDF-2 ICDD database of powder diffraction patterns. The average crystallite size was estimated by the widths of corresponding patterns using the Scherrer equation by MDI Jade® software package.

Transmission electron microscopy (TEM) and energy-dispersive X-ray spectroscopy (EDX) were carried out using FEI's Tecnai Osiris TEM equipped with X-FEG gun at 200 KeV. To obtain the microphotographs and determine particles sizes Gatan DigitalMicrograph® software was used. To analyze the average particles sizes SigmaPlot software was used.

X-ray photoelectron spectra were obtained from previously degassed under vacuum samples using an upgraded electronic spectrometer ES – 2403 SDB AI RAS equipped with a PHOIBOS 100–5MCD energy analyzer (manufactured by SpecsGmbH, Germany) and an  $\text{MgK}\alpha/\text{AlK}\alpha$  XR-50 X-ray source (manufactured by SpecsGmbH, Germany). Characteristic  $\text{MgK}\alpha$  radiation with a power of 250 W was used for photoelectron excitation for all samples. The temperature of the samples during the analysis did not exceed  $23^\circ\text{C}$ . Spectra were recorded at the pressure of no higher than  $3 \cdot 10^{-6}$  Pa. Survey spectra were obtained in the range  $1100\text{--}0$  eV with a step of 0.5 eV and an exposure at a point of 0.4 s; the transmission energy of the analyzer was 40 eV, which corresponds to 1.4 eV of the FWHM of the photoelectron band of the Ag  $3d_{5/2}$  standard. High resolution spectra were obtained with an energy step of 0.05 eV; the transmittance energy of the analyzer while recording high-resolution spectra was 7 eV, which corresponds to 0.85 eV of the FWHM of the photoelectron band of the Ag  $3d_{5/2}$  standard. Spectra were obtained using standard SpecsLab2 software. To analyze the spectra CasaXPS software package was used.

$\text{NH}_3$  temperature-programmed desorption ( $\text{NH}_3\text{-TPD}$ ) was carried out on a USGA-101 chemisorption analyzer manufactured by UNISIT (Russia). 0.15–0.20 g of a sample was placed in a quartz tube reactor. Standard automatic pretreatment included sequential operations of calcining the sample at  $500^\circ\text{C}$  for 1 h in a helium flow, saturation with  $\text{NH}_3$  at  $60^\circ\text{C}$  for 15 min, and removal of physically adsorbed  $\text{NH}_3$  in a He flow at  $100^\circ\text{C}$ . The  $\text{NH}_3\text{-TPD}$  experiment was carried out in a flow of He (30 ml/min) with a temperature rise rate of  $8^\circ/\text{min}$ . The evolved  $\text{NH}_3$  was recorded with a thermal conductivity detector.

### 3. Results and discussion

#### 3.1. Catalysts characterization

##### 3.1.1. Powder X-ray diffraction

The formation of crystalline NiP-phase was confirmed by XRD for samples generated after 6 h at  $250\text{--}350^\circ\text{C}$  for the NiP- $\text{H}_3\text{PO}_2$  and at  $300\text{--}350^\circ\text{C}$  for the NiP-TOP systems. Powder X-ray diffraction patterns of nickel phosphide were obtained for these catalysts (Fig. 1). For the NiP-TOP system samples generated at  $250^\circ\text{C}$  could not be isolated by centrifugation from the reaction medium. Thus, it can be concluded that at this temperature, the catalysts samples was amorphous. This is consistent with the literature data [13,22]. At  $300\text{--}350^\circ\text{C}$  catalysts were separated from the solution well. For the catalyst obtained at  $300^\circ\text{C}$  patterns of  $\text{Ni}_{12}\text{P}_5$  (PDF#22-1190) and  $\text{Ni}_2\text{P}_2\text{O}_7$  (PDF#74-1604) were defined. For the catalyst obtained at  $350^\circ\text{C}$   $\text{Ni}_2\text{P}$  (PDF#65-9706) patterns were defined. With increasing temperature the degree of crystallinity of a catalyst is risen,  $\text{Ni}_{12}\text{P}_5$  phase is converted into  $\text{Ni}_2\text{P}$  phase,

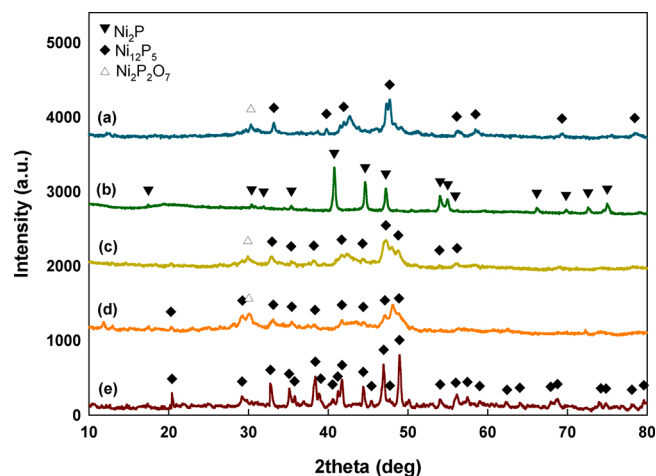


Fig. 1. The XRD patterns of nickel phosphide based catalysts generated in situ in the reaction medium during the hydrodeoxygenation of furfural (5 MPa  $\text{H}_2$ , 6 h, P/Ni ratio = 2): (a) NiP-TOP,  $300^\circ\text{C}$ , (b) NiP-TOP,  $350^\circ\text{C}$ , (c) NiP- $\text{H}_3\text{PO}_2$ ,  $250^\circ\text{C}$ , (d) NiP- $\text{H}_3\text{PO}_2$ ,  $300^\circ\text{C}$ , (e) NiP- $\text{H}_3\text{PO}_2$ ,  $350^\circ\text{C}$ .

amount of crystalline phosphate is decreased and it is not identified by XRD. In contrast to the NiP-TOP, the NiP- $\text{H}_3\text{PO}_2$  catalyst obtained at  $250^\circ\text{C}$  was isolated from the reaction medium. For the catalysts obtained at  $250^\circ\text{C}$  and  $300^\circ\text{C}$  the patterns of  $\text{Ni}_{12}\text{P}_5$  and  $\text{Ni}_2\text{P}_2\text{O}_7$  were defined. The catalyst, obtained at  $350^\circ\text{C}$ , had only the patterns of crystalline  $\text{Ni}_{12}\text{P}_5$ . Phosphate was not identified in this sample. The average sizes of crystallites for the samples obtained at  $350^\circ\text{C}$  were estimated by the width of the patterns, corresponding to (420), (312) planes in  $\text{Ni}_{12}\text{P}_5$  and (111), (201), (210) planes in  $\text{Ni}_2\text{P}$  (Table S1, Online Supplementary Material). The average crystallite sizes of  $\text{Ni}_{12}\text{P}_5$  and  $\text{Ni}_2\text{P}$  were  $33\text{--}36$  nm and  $39\text{--}47$  nm respectively.

The XRD patterns of purchased nickel phosphide that was used as a catalyst for comparative study are shown at the Fig. S1.  $\text{Ni}_2\text{P}$  (PDF#65-9706) and  $\text{Ni}_5\text{P}_4$  (PDF#18-0883) phases were identified. The average crystallite sizes were identified for (111) plane of  $\text{Ni}_2\text{P}$  and for (214) plane of  $\text{Ni}_5\text{P}_4$  and were 18 nm and 33 nm respectively.

##### 3.1.2. Transmission electron microscopy with energy-dispersive X-ray spectroscopy

The formation of nickel-phosphorus containing nanoparticles in the catalytic systems was confirmed by TEM technique for the NiP- $\text{H}_3\text{PO}_2$  and the NiP-TOP samples, obtained under different conditions. The microphotographs of the NiP- $\text{H}_3\text{PO}_2$  obtained at  $250\text{--}300^\circ\text{C}$  after 6 h of the reaction and the microphotographs of the NiP-TOP obtained at  $300^\circ\text{C}$  after 6 h of the reaction are shown in Fig. S2. For the NiP- $\text{H}_3\text{PO}_2$  sample obtained at  $250^\circ\text{C}$  particles with the average size of  $60\text{--}70$  nm are observed (Fig. S3a). There are hollow particles with the average size of  $112\text{--}147$  nm in the NiP- $\text{H}_3\text{PO}_2$  sample obtained at  $300^\circ\text{C}$ . For the NiP-TOP sample obtained at  $300^\circ\text{C}$  a small amount of hollow particles are observed. The average size of the NiP-TOP particles is  $109\text{--}129$  nm (Fig. S4c). The microphotographs of the NiP- $\text{H}_3\text{PO}_2$  obtained at  $350^\circ\text{C}$  are pictured in Fig. 2. The samples are represented by particles agglomerates. As seen in the figure, after 0.5 h the catalyst particles are inside of the shells. The average size of catalyst particles are similar and it is approximately about  $35\text{--}40$  nm (Fig. S4a). A small amount of large particles are presented in the sample. After 6 h shells are not observed. Particles have wide size distribution. In addition to medium-sized particles, large particles with the size of  $100\text{--}300$  nm are obtained. Therefore, longer reaction time leads to particles enlargement. The lattice fringes of the NiP- $\text{H}_3\text{PO}_2$  sample obtained after 6 h and line profile are presented in Fig. S5. The value of 0.234 nm is corresponded to the d-spacing of the (112) plane of  $\text{Ni}_{12}\text{P}_5$  [26,27]. The microphotographs of the NiP-TOP are pictured in Fig. 3. The formation tendency is

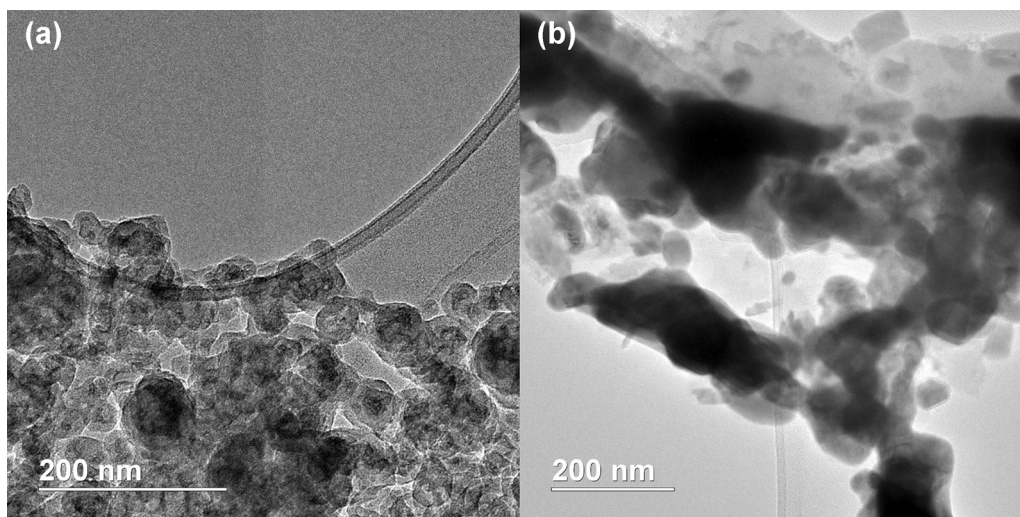


**Fig. 2.** The microphotographs of the nickel phosphide catalyst NiP-H<sub>3</sub>PO<sub>2</sub> generated in situ in the reaction medium during the hydrodeoxygenation of furfural at 350 °C a) after 0.5 h, b) after 6 h.

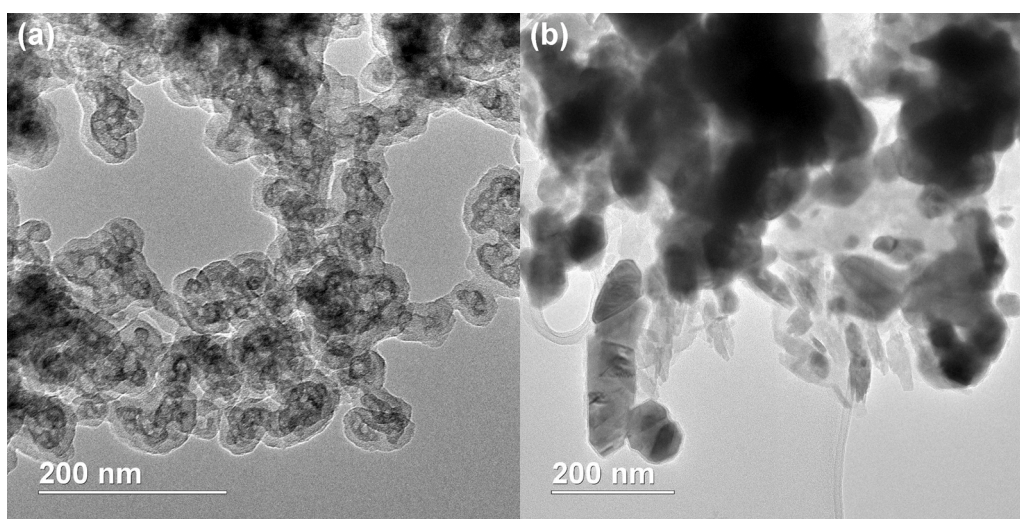


**Fig. 3.** The microphotographs of the nickel phosphide catalyst NiP-TOP generated in situ in the reaction medium during the hydrodeoxygenation of furfural at 350 °C a) after 0.5 h, b) after 6 h.

observed as well is for the NiP-H<sub>3</sub>PO<sub>2</sub>. At first, catalyst particles have shells and narrow size distribution with the average particles size about 26–30 nm (Fig. S4b), then shells are destroyed, which leads to particles enlargement and wide size distribution. Electron diffraction patterns for the NiP-TOP sample was obtained using the inverse Fourier transform of TEM images (Fig. S6). The value of 0.222 nm is corresponded to the d-spacing of (111) plane of Ni<sub>2</sub>P [28,29]. The lattice spacing values of 0.342 nm, 0.284 nm and 0.506 nm could be assigned to the (001) plane, (011) or (101) planes and (100) or (010) planes of Ni<sub>2</sub>P respectively [29–31].

According to EDX analysis, elemental maps of samples were obtained. Nickel, phosphorus and oxygen on the surface of the catalysts are observed for the NiP-H<sub>3</sub>PO<sub>2</sub> samples obtained at 250 °C (Fig. S7) and 300 °C (Fig. S8) and for the NiP-TOP sample obtained at 300 °C (Fig. S9). There is a small amount of hollow particles in the NiP-H<sub>3</sub>PO<sub>2</sub> sample obtained at 250 °C, which was not observed by TEM technique. The Fig. S8 confirmed that hollow particles contains in the NiP-H<sub>3</sub>PO<sub>2</sub> sample obtained at 300 °C. For the NiP-TOP sample obtained at 300 °C. For the NiP-H<sub>3</sub>PO<sub>2</sub> sample after 0.5 h of the reaction at 3 μm of scale nickel and phosphorus were located in the same areas for all particles of

the sample besides large ones (Fig. S10). When zoomed up to 200 nm, it was seen, that nickel and phosphorus in large particles were located in the same areas as well as for others (Fig. S11). There are areas in which phosphorus is located with oxygen, and nickel is absent. It can be concluded that there is phosphorus- and oxygen-containing compound. Particles shells, which were obtained by TEM, are amorphous and consist of carbon-containing compounds (Fig. S12). It can be assumed that shells are formed by adsorption of ligands. During the reaction process shells are destroyed because compounds, containing in the systems, are underwent changes. The NiP-TOP elemental maps after 0.5 h of the reaction are showed in Fig. S13-S14. For the NiP-H<sub>3</sub>PO<sub>2</sub> after 6 h of the reaction nickel and phosphorus were located in the same areas (Fig. S15). Oxygen containing in the sample is observed on the surface of the catalyst. It can be related to unreduced or oxidized P—OH groups, which were mentioned earlier [10,32–34]. For the NiP-TOP catalyst a similar situation is observed (Fig. S16).

### 3.1.3. X-ray photoelectron spectroscopy

The XPS spectra of the NiP-H<sub>3</sub>PO<sub>2</sub> (Fig. S17) and the NiP-TOP (Fig. S18) samples obtained at 350 °C after 6 h of the reaction were

measured to identify the surface chemical composition and valence states. The XPS survey spectrum of the NiP-H<sub>3</sub>PO<sub>2</sub> (Fig. S17a) shows the presence of Ni, P, O, C elements. The XPS survey spectrum of the NiP-TOP (Fig. S18a) shows the presence of Ni, P, O, C and Fe elements. The impurity of Fe could be explained by leaching of reactor material under the reaction conditions. The XPS spectra shows Ni and P reduced and oxidized species related to nickel phosphide and nickel phosphate respectively. It is suggested that small positive charge of Ni and small negative charge of P occur due to electron density transfer from Ni to P [35]. The magnitude of Ni changes as follows: Ni<sub>2</sub>P > Ni<sub>12</sub>P<sub>5</sub> > Ni [36, 37]. However, it cannot be reliably stated, which phase of phosphide was formed, with slight differences in the binding energy values. The values of 853.5 eV and 853.7 eV of binding energy are corresponded to Ni<sup>δ+</sup> chemical state in nickel phosphide in the NiP-H<sub>3</sub>PO<sub>2</sub> (Fig. S17b) and NiP-TOP (Fig. S18b) respectively [30]. Binding energies of 857.1 and 856.8 eV refer to nickel in the oxidized state which can be associated with nickel phosphate in the NiP-H<sub>3</sub>PO<sub>2</sub> and the NiP-TOP respectively [30,36,37]. Binding energies of 862.2 and 862.1 eV refer to shake-up satellite of Ni<sup>2+</sup> in Ni<sub>2p/3</sub> region in the NiP-H<sub>3</sub>PO<sub>2</sub> and the NiP-TOP respectively [30,36,37]. The peaks observed at 129.7 eV and 129.9 eV are attributed to P<sup>δ-</sup> in the NiP-H<sub>3</sub>PO<sub>2</sub> and the NiP-TOP respectively. Binding energies of 129.7 eV and 133.7 eV in NiP-H<sub>3</sub>PO<sub>2</sub> are corresponded to P<sup>δ-</sup> in phosphide and P<sup>5+</sup> species related to phosphate (Fig. S17c). Binding energies of 129.9 eV and 133.8 eV in the NiP-TOP are also related to reduced P<sup>δ-</sup> and oxidized P<sup>5+</sup> species (Fig. S18c) [35].

### 3.1.4. NH<sub>3</sub> temperature-programmed desorption

The NH<sub>3</sub>-TPD desorption curves of the NiP-H<sub>3</sub>PO<sub>2</sub> and the NiP-TOP samples obtained at 350 °C after 6 h are presented in Fig. S19. For both of the catalysts only the weak acid sites were detected. It was assigned to the P—OH groups [38]. The desorption peak for the NiP-H<sub>3</sub>PO<sub>2</sub> and NiP-TOP catalysts was observed at around 168 °C and 138 °C respectively. The amount of the desorbed ammonia was 45 and 6 μmol/g respectively. Thus, the NiP-H<sub>3</sub>PO<sub>2</sub> acidity was higher than the NiP-TOP acidity. It can be due to the fact that acidic component was involved to the synthesis of the NiP-H<sub>3</sub>PO<sub>2</sub> and only neutral components were involved to the synthesis of the NiP-TOP. Nickel phosphate is formed as a by-product of the hypophosphorous acid decomposition [39] and contributes to the higher acidity of the NiP-H<sub>3</sub>PO<sub>2</sub> sample compared to the NiP-TOP.

### 3.2. Hydrogenation of furfural

Mentioned catalytic systems were tested in the hydrodeoxygenation of furfural. Earlier similar systems were successfully tested in the hydrodeoxygenation of guaiacol [14], palmitic and stearic acids [15]. In present work, the first catalytic system consists of Ni (II) 2-ethylhexanoate and TOP, furfural as a substrate and toluene as a solvent (the NiP-TOP series of catalysts were obtained), the second catalytic system consists of Ni(OAc)<sub>2</sub>, H<sub>3</sub>PO<sub>2</sub>, furfural and ethanol (the NiP-H<sub>3</sub>PO<sub>2</sub> series of catalysts were obtained). Both of systems were active in the hydro-processing of furfural. Type of reaction products and their distribution firstly depended on used catalytic system and solvent, secondly on reaction temperature and time. The transformations occurring with furfural and its derivatives using the catalytic systems proceed with the participation of metal and acid sites. Ni in Ni<sub>2</sub>P is responsible for transformations over metal sites. P—OH groups on the catalyst surface and in H<sub>3</sub>PO<sub>2</sub> are Brønsted acid sites [32,40]. Ni<sup>2+</sup> and Ni<sup>δ+</sup> are Lewis acid sites [35,40,41].

Mavrikakis and Barteau were reported about two types of intermediates, formed on the metal surface as a result of aldehyde adsorption. η<sup>1</sup>(O) aldehyde intermediate configuration is bonded to the surface via oxygen atom, η<sup>2</sup>(C,O) aldehyde intermediate configuration is bonded via carbon and oxygen atoms [42]. η<sup>2</sup>(C,O) intermediate is more stable and it is typical for the adsorption on the Ni-containing surface. This intermediate can be converted into furfuryl alcohol by

hydrogenation and into furan by decarbonylation [18,43]. For the NiP-TOP two routes of furfural conversion are observed. The results of catalytic tests of the NiP-TOP are presented in Fig. 4. Proposed reaction pathways are presented in Fig. 5. Furan was obtained from furfural at all reaction temperatures over metal sites of catalyst. With increasing temperature, the furan selectivity decreased. The highest selectivity for furan was 44 % at 250 °C after 3 h of reaction. Furfuryl alcohol was an intermediate product and was converted into 2-methylfuran over metal sites by hydrogenolysis [44]. 2-methylfuran was a main product at all temperatures and reaction time. Thus, the conversion to furfuryl alcohol prevailed and with increasing temperature the conversion to furan was inhibited more. Full conversion of furfural reached after 3 h at 250 °C, after 1 h at 300 °C and after 0.5 h at 350 °C. With increasing temperature 2-pentanone was detected among the reaction products. It was generated from 2-methylfuran by ring-opening hydrogenation reaction over metal sites [45]. The highest selectivity of 2-methylfuran were 77 % at 350 °C after 3 h of the reaction. Jimenez-Gomez et al. [18] reported about the obtaining of 2-methylfuran and furan among the reaction products with 75.4 % and 24.5 % of selectivity respectively over Ni<sub>2</sub>P/SiO<sub>2</sub> at 190 °C at full conversion. However, with increasing temperature to 210 °C 2-methylfuran selectivity decreased to 15.8 %, furan selectivity increased to 44.7 % and tetrahydrofuran was obtained with 38.4 % of selectivity.

The results of catalytic tests of the NiP-H<sub>3</sub>PO<sub>2</sub> are presented in Fig. 6. Product selectivity in ethanol as a solvent was lower than in toluene. It can be explained by the presence of numerous competing reactions. Proposed reaction pathways are presented in Fig. 7. Furfuryl alcohol was the one product formed from furfural in the first stage. Thus, furfural decarbonylation to furan in ethanol was totally inhibited. Products with the highest selectivity of 40 % and 38 % in ethanol were ethyl levulinate and 2-methylfuran respectively. Full conversion of furfural reached after 1 h at 250 °C and 300 °C and after 0.5 h at 350 °C. Ethyl levulinate was obtained from furfuryl alcohol by Brønsted acid-catalyzed ring-opening hydrogenation and following esterification [46,47]. It was mentioned about acid-catalyzed conversion of furfural into ethyl levulinate [48, 49]. Apparently it also happens through furfuryl alcohol formation catalyzed by Lewis acid sites [47]. With increasing temperature γ-valerolactone and ethyl valerate were detected in the reaction medium. Ethyl valerate selectivity was higher than γ-valerolactone selectivity. There are two possible pathways of ethyl levulinate conversion into γ-valerolactone. The first is the formation of angelica lactone as an intermediate product by the deethoxylation over Lewis acid sites and following hydrogenation over metal sites. The second is the formation of ethyl 2-hydroxyvalerate over metal or Lewis acid sites and following deethoxylation over Lewis acid sites [50,51]. Hydrogenolysis of ethyl 2-hydroxyvalerate into ethyl valerate is proceeded over metal sites [51]. The conversion of γ-valerolactone into ethyl valerate which is catalyzed by Brønsted acid sites is proceeded through the formation of ethyl pentenoate [52]. The highest value for ethyl valerate was 26 % and was obtained after 6 h of the reaction at 350 °C. Tetrahydro-2-methylfuran could be obtained from 2-methylfuran by hydrogenation, from tetrahydrofurfuryl alcohol by hydrogenolysis and from γ-valerolactone by hydrodeoxygenation [53]. However, tetrahydrofurfuryl alcohol was not detected among the reaction products. The pattern of γ-valerolactone transformation into tetrahydro-2-methylfuran is not traced in present work. Thus, tetrahydro-2-methylfuran was obtained from 2-methylfuran by hydrogenation over metal sites [43]. With increasing reaction time selectivity of tetrahydro-2-methylfuran increased and the highest value of 33 % was obtained at 300 °C after 6 h of the reaction. Moreover, 2-(diethoxymethyl)furan and 5,5-diethoxy-2-pentanone were detected in the reaction medium. They are acetals of ethanol with furfural and 4-oxopentanal respectively [54]. 4-oxopentanal could be obtained by hydrogenation of carboxylic group in levulinic acid, but it was not detected among the products. With increasing temperature the yields of acetals increased first, and then decreased. These acetals were formed over Brønsted or Lewis acid sites of catalyst [54–56]. In addition,

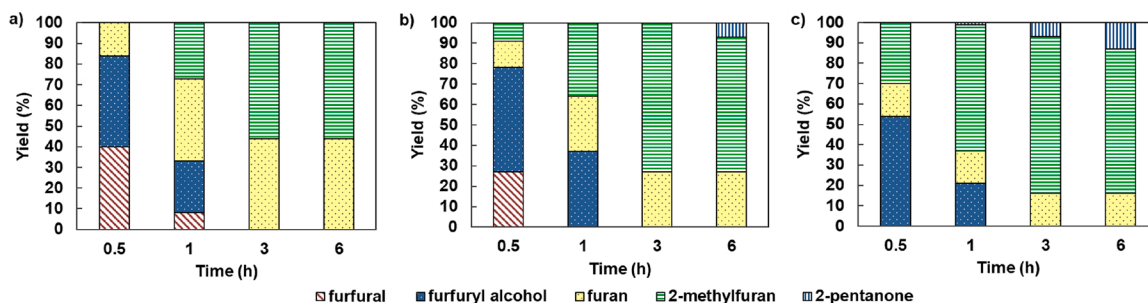


Fig. 4. Catalytic activity tests of the NiP-TOP. Furfural was used as a substrate, toluene was used as a solvent. Reaction conditions: 5 MPa H<sub>2</sub>, 0.5-6 h, a) 250 °C, b) 300 °C, c) 350 °C.

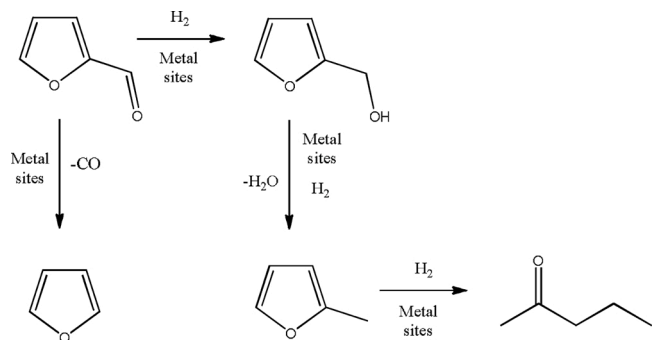


Fig. 5. Proposed reaction pathways of furfural hydrodeoxygenation in toluene over in situ generated nickel phosphide based catalyst.

2-pentanone was obtained among the products. With increasing reaction time 2-pentanone selectivity increased and the highest selectivity was 24 % at 350 °C after 6 h of the reaction. 2-pentanone was produced from 2-methylfuran by ring-opening hydrogenation over metal sites [45], from ethyl levulinate by desterification over Brønsted acid sites [47] and following hydrogenation over metal sites, from 5,5-diethoxy-2-pentanone by deacetalization over Brønsted or Lewis acid sites and following hydrogenation over metal sites. The highest selectivity for 2-methylfuran were 36 % and 38 % at 250 °C and 350 °C respectively after 1 h of the reaction. The highest selectivity for ethyl levulinate were 39 % and 40 % at 250 °C and 350 °C respectively after 3 h of the reaction. Among the products furfuryl alcohol, 2-methylfuran and 2-pentanone were detected both in polar and non-polar media. Unlike toluene, ethanol was involved in the products formation. Ring-opening products were obtained after 0.5 h of the reaction using ethanol as a solvent. Using toluene, it was happened later and at higher temperature. The one ring-opening product in toluene was 2-pentanone. Besides 2-pentanone, ethyl levulinate and ethyl valerate were obtained in ethanol. Lee and Chen [20] reported about 80 % of furfuryl alcohol

selectivity in hydroprocessing of furfural using ethanol as a solvent and unsupported Ni<sub>2</sub>P as a catalyst. In addition, they obtained tetrahydrofurfuryl alcohol. Santana Krishnan et al. [19] obtained 67.6 % of 2-propoxymethylfuran selectivity using 2-propanol as a solvent and MoS catalyst, modified by NiP and laponite as a support. Other products were tetrahydrofuran, tetrahydro-2-methylfuran and 2-methylfuran. Thus, reactions proceeding with the use of NiP-based catalytic systems and ethanol as a solvent in present work differed from the reactions described in the literature earlier.

### 3.3. Recycling catalytic test and comparative study with commercial catalyst

The influence of Ni(OAc)<sub>2</sub> and H<sub>3</sub>PO<sub>2</sub> separately on the reaction products was investigated previously in the HDO of guaiacol [14]. It was shown, that conversion of guaiacol and the reaction products selectivity differed for Ni(OAc)<sub>2</sub>, H<sub>3</sub>PO<sub>2</sub> and nickel phosphide based catalyst, generated in situ. Nickel phosphide based catalyst made the greatest contribution to the HDO of guaiacol. The situation was similar for furfural. Recycling catalytic tests were carried out to prove it. At full conversion in the presence of the NiP-TOP system, the selectivity changed insignificantly (Fig. S20). The selectivity of 2-pentanone slightly decreased, while the selectivity of 2-methylfuran slightly increased. At medium values of transformation, decrease of conversion (Fig. S21) and selectivity (Fig. S22) was more noticeable. The conversion decreased slowly. After 13th test run furan was not observed among the reaction products.

At full conversion in the presence of the NiP-H<sub>3</sub>PO<sub>2</sub> system, the selectivity changed insignificantly (Fig. S23). The selectivity of 2-methylfuran and ethyl levulinate slightly increased while the selectivity of other products slightly decreased. As well as in the presence of the NiP-TOP system at medium values of transformation decrease of conversion (Fig. S24) and selectivity (Fig. S25) was noticeable. First, in the presence of the NiP-H<sub>3</sub>PO<sub>2</sub> products such as acetals (which synthesis was catalyzed only by H<sub>3</sub>PO<sub>2</sub>) were not formed. Therefore, the conversion

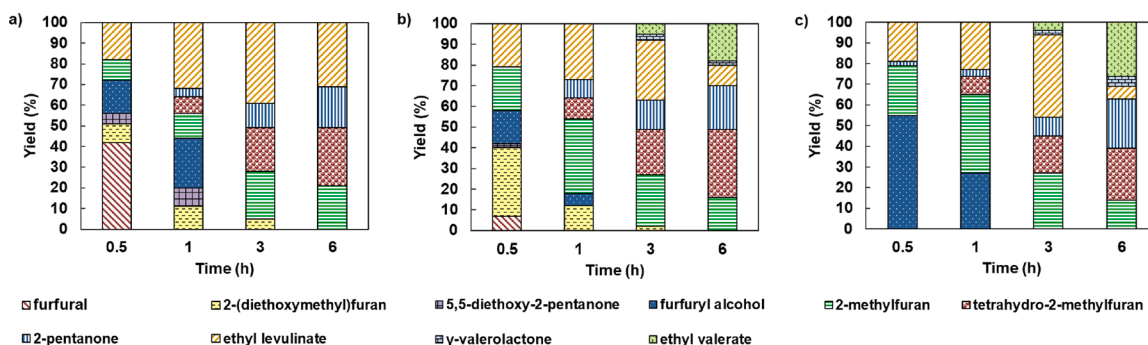


Fig. 6. Catalytic activity tests of the NiP-H<sub>3</sub>PO<sub>2</sub>. Furfural was used as a substrate, ethanol was used as a solvent. Reaction conditions: 5 MPa H<sub>2</sub>, 0.5-6 h, a) 250 °C, b) 300 °C, c) 350 °C.



Shubnikov Institute of Crystallography for TEM analysis.

## Appendix A. Supplementary data

Supplementary material related to this article can be found, in the online version, at doi:<https://doi.org/10.1016/j.apcata.2020.117890>.

## References

- [1] G. Sorda, M. Banse, C. Kemfert, *Energy Policy* 38 (2010) 6977–6988, <https://doi.org/10.1016/j.enpol.2010.06.066>.
- [2] C. Shekhar, *Chem. Biol.* 18 (2011) 1199–1200, <https://doi.org/10.1016/j.chembiol.2011.10.010>.
- [3] A.S. Mammam, J.-M. Lee, Y.-C. Kim, I.T. Hwang, N.-J. Park, Y.K. Hwang, J.-S. Chang, J.-S. Hwang, *Biofuel Bioprod. Biorefin.* 2 (2008) 438–454, <https://doi.org/10.1002/bbb.95>.
- [4] Y. Luo, Z. Li, X. Liu, J. Fan, J.H. Clark, *Catal. Today* 319 (2019) 14–24, <https://doi.org/10.1016/j.cattod.2018.06.042>.
- [5] J.-P. Mikkola, E. Sklavounos, A.W.T. King, P. Virtanen, in: R. Bogel-Lukasik (Ed.), *Ionic Liquids in the Biorefinery Concept: Challenges and Perspectives*, The Royal Society of Chemistry, Cambridge, UK, 2015, pp. 1–37, <https://doi.org/10.1039/9781782622598-00001>.
- [6] J.-P. Lange, E. Heide, J. Buijtenen, R. Price, *ChemSusChem* 5 (2012) 150–166, <https://doi.org/10.1002/cssc.201100648>.
- [7] D.M. Alonso, S.G. Wettstein, J.A. Dumesic, *Green Chem.* 15 (2013) 584–595, <https://doi.org/10.1039/c3gc37065h>.
- [8] S. Carencio, I. Resa, X. Le Goff, P. Le Floch, N. Mézailles, *Chem. Commun.* (2008) 2568–2570, <https://doi.org/10.1039/b802454e>.
- [9] S.T. Oyama, *J. Catal.* 216 (2003) 343–352, [https://doi.org/10.1016/S0021-9517\(02\)00069-6](https://doi.org/10.1016/S0021-9517(02)00069-6).
- [10] M.E. Bussell, *Chem. Eng.* 2 (2017) 628–635, <https://doi.org/10.1039/c7re00098g>.
- [11] A.-M. Alexander, J.S.J. Hargreaves, *Chem. Soc. Rev.* 39 (2010) 4388–4401, <https://doi.org/10.1039/b916787k>.
- [12] S.T. Oyama, T. Gott, H. Zhao, Y.-K. Lee, *Catal. Today* 143 (2009) 94–107, <https://doi.org/10.1016/j.cattod.2008.09.019>.
- [13] J. Wang, A.C. Johnston-Peck, J.B. Tracy, *Chem. Mater.* 21 (2009) 4462–4467, <https://doi.org/10.1021/cm901073k>.
- [14] M.A. Golubeva, A.L. Maximov, *Mendeleev Commun.* 29 (2019) 550–552, <https://doi.org/10.1016/j.mencom.2019.09.024>.
- [15] M.A. Golubeva, A.L. Maksimov, *Pet. Chem.* 59 (2019) 1326–1330, <https://doi.org/10.1134/s0965544119120041>.
- [16] Y. Wang, F. Liu, H. Han, L. Xiao, W. Wu, *ChemistrySelect* 3 (2018) 7926–7933, <https://doi.org/10.1002/slct.201800929>.
- [17] Y. Wang, X. Feng, S. Yang, L. Xiao, W. Wu, *J. Nanopart. Res.* 22 (2020) 67–80, <https://doi.org/10.1007/s11051-020-04784-z>.
- [18] C.P. Jiménez-Gómez, J.A. Cecilia, R. Moreno-Tost, P. Maireles-Torres, *ChemCatChem* 9 (2017) 2881–2889, <https://doi.org/10.1002/cctc.201700312>.
- [19] P. Santana Krishnan, P. Tamizhdurai, A. Alagarasi, K. Shanthi, *Int. J. Hydrog. Energy.* 44 (2019) 14968–14980, <https://doi.org/10.1016/j.ijhydene.2019.04.153>.
- [20] S.-P. Lee, Y.-W. Chen, *Ind. Eng. Chem. Res.* 38 (1999) 2548–2556, <https://doi.org/10.1021/ie990071a>.
- [21] T. Herman, S. Soden, *AIP Conf. Proc.* 166 (1988) 99–108, <https://doi.org/10.1063/1.37136>.
- [22] E. Muthuswamy, G.H.L. Savithra, S.L. Brock, *ACS Nano* 5 (2011) 2402–2411, <https://doi.org/10.1021/nn1033357>.
- [23] Y.Y. Dou, G.R. Li, J. Song, X.P. Gao, *Phys. Chem. Chem. Phys.* 14 (2012) 1339–1342, <https://doi.org/10.1039/c2cp23775j>.
- [24] H. Dong, S. Hong, Y. Zuo, X. Zhang, Z. Lu, J. Han, L. Wang, L. Ni, C. Li, Y. Wang, *ChemCatChem* 11 (2019) 6263–6269, <https://doi.org/10.1002/cctc.201901618>.
- [25] X. Zhang, Y. Liu, Q. Xiong, G. Liu, C. Zhao, G. Wang, Y. Zhang, H. Zhang, H. Zhao, *Electrochim. Acta* 254 (2017) 44–49, <https://doi.org/10.1016/j.electacta.2017.09.097>.
- [26] L. Feng, H. Vruble, M. Bensimon, X. Hu, *Phys. Chem. Chem. Phys.* 16 (2014) 5917–5921, <https://doi.org/10.1039/c4cp00482e>.
- [27] I.I. Abu, K.J. Smith, *J. Catal.* 241 (2006) 356–366, <https://doi.org/10.1016/j.jcat.2006.05.010>.
- [28] X. Wang, Y.V. Kolen'ko, L. Liu, *Chem. Commun.* 51 (2015) 6738–6741, <https://doi.org/10.1039/c5cc00370a>.
- [29] I.I. Abu, K.J. Smith, *Appl. Catal. A* 328 (2007) 58–67, <https://doi.org/10.1016/j.apcata.2007.05.018>.
- [30] J.A. Cecilia, A. Infantes-Molina, E. Rodríguez-Castellón, A. Jiménez-López, S. T. Oyama, *Appl. Catal. B* 136–137 (2013) 140–149, <https://doi.org/10.1016/j.apcatb.2013.01.047>.
- [31] I.V. Delyi, I.V. Shamanaev, E.Y. Gerasimov, V.P. Pakharukova, I.V. Yakovlev, O. B. Lapina, P.V. Aleksandrov, G.A. Bukhtiyarova, *Catalysts* 7 (2017) 298–318, <https://doi.org/10.3390/catal7100298>.
- [32] R. Wang, K.J. Smith, *Appl. Catal. A* 380 (2010) 149–164, <https://doi.org/10.1016/j.apcata.2010.03.055>.
- [33] Y. Pan, Y. Liu, J. Zhao, K. Yang, J. Liang, D. Liu, W. Hu, D. Liu, Y. Liu, C. Liu, J. Mater. Chem. A 3 (2015) 1656–1665, <https://doi.org/10.1039/c4ta04867a>.
- [34] W. Zhou, H. Xin, H. Yang, X. Du, R. Yang, D. Li, C. Hu, *Catalysts* 8 (2018) 153–172, <https://doi.org/10.3390/catal8040153>.
- [35] M. Peroni, I. Lee, X. Huang, E. Baráth, O.Y. Gutiérrez, J.A. Lercher, *ACS Catal.* 7 (2017) 6331–6341, <https://doi.org/10.1021/acscatal.7b01294>.
- [36] D. Liu, A. Wang, C. Liu, R. Prins, *Catal. Today* 292 (2017) 133–142, <https://doi.org/10.1016/j.cattod.2016.09.019>.
- [37] Y.-K. Lee, S.T. Oyama, *J. Catal.* 239 (2006) 376–389, <https://doi.org/10.1016/j.jcat.2005.12.029>.
- [38] K. Li, R. Wang, J. Chen, *Energy Fuels* 35 (2011) 854–863, <https://doi.org/10.1021/ef101258j>.
- [39] M. Mavrikakis, M.A. Barteau, *J. Mol. Catal. A Chem.* 131 (1998) 135–147, [https://doi.org/10.1016/S1381-1169\(97\)00261-6](https://doi.org/10.1016/S1381-1169(97)00261-6).
- [40] S. Sitthisa, D.E. Resasco, *Catal. Lett.* 141 (2011) 784–791, <https://doi.org/10.1007/s10562-011-0581-7>.
- [41] S. Sitthisa, W. An, D.E. Resasco, *J. Catal.* 284 (2011) 90–101, <https://doi.org/10.1016/j.jcat.2011.09.005>.
- [42] C.L. Wilson, *J. Am. Chem. Soc.* 70 (1948) 1313–1315, <https://doi.org/10.1021/ja01184a006>.
- [43] G.M. González Maldonado, R.S. Assary, J.A. Dumesic, L.A. Curtiss, *Energy Environ. Sci.* 5 (2012) 8990–8997, <https://doi.org/10.1039/c2ee22486k>.
- [44] Y. Shao, K. Sun, L. Zhang, Q. Xu, Z. Zhang, Q. Li, S. Zhang, Y. Wang, Q. Liu, X. Hu, *Green Chem.* 21 (2019) 6634–6645, <https://doi.org/10.1039/c9gc03056e>.
- [45] L. Peng, L. Lin, J. Zhang, J. Shi, S. Liu, *Appl. Catal. A* 397 (2011) 259–265, <https://doi.org/10.1016/j.apcata.2011.03.008>.
- [46] C. Chang, G. Xu, W. Zhu, J. Bai, S. Fang, *Fuel* 140 (2015) 365–370, <https://doi.org/10.1016/j.fuel.2014.09.102>.
- [47] L. Bui, H. Luo, W.R. Gunther, Y. Román-Leshkov, *Angew. Chem.* 125 (2013) 8180–8183, <https://doi.org/10.1002/ange.201302575>.
- [48] V. Mohan, V. Venkateshwarlu, C.V. Pramod, B.D. Raju, K.S.R. Rao, *Catal. Sci. Technol.* 4 (2014) 1253–1259, <https://doi.org/10.1039/c3cy01072d>.
- [49] N. Karanwal, D. Verma, P. Butolia, S.M. Kim, J. Kim, *Green Chem.* 22 (2020) 766–787, <https://doi.org/10.1039/c9gc03516h>.
- [50] I. Obregón, I. Gandarias, M.G. Al-Shaal, C. Mevissen, P.L. Arias, R. Palkovits, *ChemSusChem* 9 (2016) 2488–2495, <https://doi.org/10.1002/cssc.201600751>.
- [51] P. Neves, S. Lima, M. Pillinger, S.M. Rocha, J. Rocha, A.A. Valente, *Catal. Today* 218–219 (2013) 76–84, <https://doi.org/10.1016/j.cattod.2013.04.035>.
- [52] Z. Babaei, A.N. Chermahini, M. Dinari, *Chem. Eng.* 352 (2018) 45–52, <https://doi.org/10.1016/j.cej.2018.07.004>.
- [53] M.J. da Silva, M. Galdino Teixeira, *Mol. Catal.* 461 (2018) 40–47, <https://doi.org/10.1016/j.mcat.2018.10.002>.
- [54] P. Panagiotopoulou, N. Martin, D.G. Vlachos, *J. Mol. Catal. Chem.* 392 (2014) 223–228, <https://doi.org/10.1016/j.molcata.2014.05.016>.
- [55] G. Morales, J.A. Melero, J. Iglesias, M. Paniagua, C. López-Aguado, *React. Chem. Eng.* 4 (2019) 1834–1843, <https://doi.org/10.1039/c9re00117d>.